Communications in Computational Chemistry
Commun. Comput. Chem., Vol. 1, No. 1, 61–70
doi: 10.4208/cicc.2025.71.01
Regular Article

First Theoretical Evidence of Blue-Shifted Energy Transfer in Bioluminescence

Shuangqi Pi[1], Yanling Luo[2], Deping Hu[1,*] and Ya-Jun Liu[1,3,*]

[1] *Department of Chemistry, Faculty of Arts and Sciences, Center for Advanced Materials Research, Beijing Normal University, Zhuhai 519087, China;*
[2] *School of Chinese Materia Medica, Tianjin University of Traditional Chinese Medicine, Tianjin 301617, China;*
[3] *Key Laboratory of Theoretical and Computational Photochemistry, Ministry of Education, College of Chemistry, Beijing Normal University, Beijing 100875, China.*

[*] Corresponding authors: depinghu@bnu.edu.cn, pisq@bnu.edu.cn

Received on 12 March 2025; Accepted on 07 April 2025

Abstract: Energy transfer (ET) complex is not rare in bioluminescence. Usually, the ET occurs from the donor with higher emission energy to the acceptor with lower absorption energy. However, a blue-shifted ET is observed in the bioluminescence (BL) of *Photobacterium phosphoreum* (*PP*). The luminophore, 4a-hydroxy-5-hydro-flavin mononucleotide at the first singlet excited state (S_1-HFOH), in solitary *PP* luciferase (*PP*Luc) emits light at 495 nm. When a proportional concentration of lumazine protein (LumP) with a substrate of 6,7-dimethyl-8-ribityllumazine (DLZ) is introduced, the emission wavelength changes to 475 nm, accompanied by a 2.1-fold enhancement in intensity. The blueshift is only an observation, whose ET mechanism has not been uncovered over fifty years of research. In the present article, we evidenced that the ET process occurs via a Förster resonance energy transfer (FRET) mechanism by protein-protein docking and molecular dynamics (MD) simulations. Moreover, utilizing the combined quantum mechanics and molecular mechanics (QM/MM) method, we calculated the FRET rate and fluorescence quantum yield. The small Stokes shift of DLZ as well as the strong vibronic couplings of HFOH allow the blue-shifted FRET process. The calculated FRET rate is larger than the radiative and non-radiative decay ones of S_1-HFOH, and the fluorescence quantum yield of S_1-DLZ is higher than the one of S_1-HFOH, which clearly explains the experimentally observed enhancement of the emission intensity. Simultaneously, the blue-shifted FRET mechanism firstly interpreted that the wild-type *PP* emits 475 nm BL rather than 490 nm one as the other species of bioluminescent bacteria do. This first-time deep investigation establishes a theoretical research paradigm for the theoretical study of ET and holds significance in color regulation in the BL field.

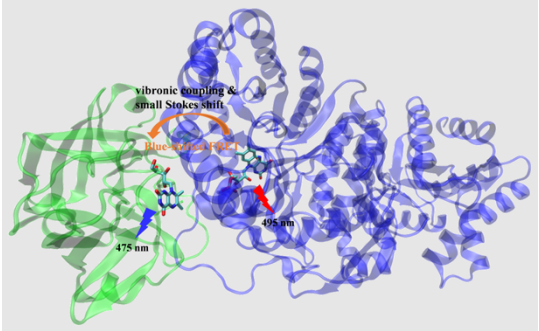

Key words: Bacterial bioluminescence, Blue shift, FRET, QM/MM, MD.

1. Introduction

The phenomenon of bioluminescence (BL) is widespread in marine and terrestrial organisms [1], and has been applied in fluorescent probes, medical research, environmental monitoring and so on [2-5]. Among them, the bacterial BL is specially used for real-time in vivo imaging due to the low cost and simple operation [6]. It was widely accepted that all bioluminescent bacteria emit BL through the same mechanism in the bacterial luciferase [7-9]. As described in Scheme 1a, the reaction process includes five stages: the reduced flavin mononucleotide anion ($FMNH^-$) reacts with oxygen to produce 4a-hydroperoxy-5-hydro-FMN (HFOOH); HFOOH reacts with the long-chain aliphatic aldehyde (RCHO) to yield 4a-peroxyhemiacetal-5-hydro-FMN [HFOOCH(OH)R]; HFOOCH(OH)R dissociates to generate the first singlet excited state (S_1-state) 4a-hydroxy-5-hydro-FMN (S_1-HFOH) and carboxylic acid (RCOOH); the bioluminophore S_1-HFOH deexcites to HFOH and emits light [10, 11]; HFOH dehydrates and transforms into flavin mononucleotide (FMN). Most of the known over 30 species of bioluminescent bacteria emit BL of wavelength around 490 nm [12,13]. However, the BL wavelength of *Photobacterium phosphoreum* (*PP*) is 475 nm [9,10]. The BL of 475 nm wavelength is not emitted by the S_1-HFOH in the *PP* luciferase (*PP*Luc), but by the S_1-state 6,7-dimethyl-8-ribityllumazine (DLZ) [14] [see Scheme 1(b)] in an antenna protein, Lumazine Protein (*PP*LumP) [15-17]. The experiments found that S_1-HFOH in solitary *PP*Luc has a maximum BL wavelength at 495 nm [9, 18]. When *PP*LumP is added, the maximum emission wavelength changes to 475 nm [19] accompanied by an enhanced intensity [18]. The extent of intensity enhancement is related to the concentration of the added *PP*LumP. Specifically, when the concentration of the added *PP*LumP is equal to that of *PP*Luc, the BL intensity increases by approximately 2.1-fold (as shown in Table 3 of ref 16) [16]. Lee et al. believed that the 20 nm blueshift is caused by an energy transfer (ET) taking place from HFOH in *PP*Luc to DLZ in *PP*LumP [20]. After more than fifty years of research, the ET mechanism is still unclear. It is difficult to obtain the complex structure of *PP*Luc and *PP*LumP by using the X-ray diffraction or nuclear magnetic resonance (NMR) spectroscopy [10], since the interaction time between energy donor protein (*PP*Luc) and energy acceptor protein (*PP*LumP) is very short.

The purpose of the present study is to investigate the blue-shifted ET mechanism with the aid of computational chemistry. We comprehensively applied the protein-protein docking, molecular dynamics (MD) simulations and combined quantum mechanics and molecular mechanics (QM/MM) calculations to thoroughly understand the ET mechanism. By reason of mechanistic similarity, the current research is helpful to understand the photosynthesis process of plant [21] and apply the technology of bioluminescence resonance ET (BRET) [22].

2. Theoretical Method

2.1 Computational systems

Originally, we intended to study the ET from HFOH in *PP*Luc to DLZ in *PP*LumP. However, both the crystal structures of *PP*Luc and *PP*LumP have not yet been obtained experimentally. The amino acid sequence of *Photobacterium kishitanii* LumP (*PK*Lump, PDB: 3A3G)

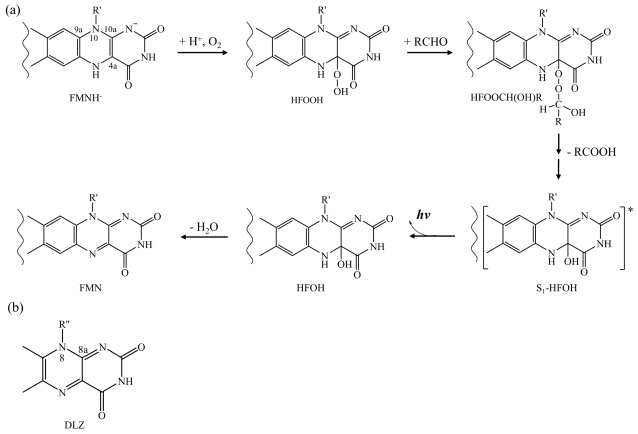

Scheme 1. (a) The rough reaction process in bacterial BL. R and R′ represent long-chain aliphatic hydrocarbons and $CH_2(CHOH)_3OPO_3H_2$ respectively. (b) The structure of 6,7-dimethyl-8-ribityllumazine (DLZ). R″ represents $CH_2(CHOH)_3CH_2OH$.

[23] is identical to that of *PP*LumP (Figure S1). The amino acid sequence of α subunit of *Vibrio harveyi* luciferase (*VH*Luc, PDB: 3FGC) [24] has 59.6% identity and 74.1% similarity with that of *PP*Luc [Figure S2 (a)]. For β subunit, the amino acid sequence of *VH*Luc has 47.6% identity and 67.5% similarity with that of *PP*Luc (Figure S2 (b)). Additionally, the predicted structure of *PP*Luc using the SWISS MODEL server [25-27] is found to closely resemble the structure of *VH*Luc [Figure S2 (c)]. As experiments evidenced, *PP*LumP forms 1:1 complex with VHLuc [28]. The addition of *PP*LumP shifts the BL in *VH*Luc at 485 nm to 475 nm [29]. Therefore, it is reasonable to replace *PP*Luc by *VH*Luc (3FGC) and *PP*LumP by *PK*LumP (3A3G). In other words, in this article, to uncover the ET mechanism in *PP* BL, we should study the ET from HFOH in *PP*Luc to DLZ in *PK*LumP, but for computational convenience, we reasonably replace the study on this ET by the study on the ET from HFOH in *VH*Luc to DLZ in *PK*LumP.

2.2 *VH*Luc-*PK*LumP docking and MD simulations

Before MD simulations, we used the ModLoop server to model the missing loop residues 284-289 in *VH*Luc and 87-93 in *PK*LumP [30, 31]. Subsequently, 10 ns MD simulations were performed for HFOH-*VH*Luc and DLZ-*PK*LumP, respectively. Finally, in the equilibrated region of the MD trajectories, the equilibrated HFOH-*VH*Luc and DLZ-*PK*LumP structures were used to perform protein-protein docking by the PatchDock [32]. The FireDock was used to refine the docked models [33]. Among the top ten protein-protein complex, one with the closest distance between DLZ and HFOH (about 18 Å) was selected for subsequent 100 ns MD simulation. For convenience, we refer to the obtained protein-protein complex as the *VH*Luc-*PK*LumP. The RMS derivation analyses were presented in Figures S3, S4 and S5. The MD simulation is in the periodic boundary conditions at constant temperature of 300 K and pressure of 1 atm via the Amber16 package [34]. The time step was 2 fs. For the details of protein-protein docking and MD simulation, see SI.

2.3 QM calculations

DOI https://doi.org/10.4208/cicc.2025.71.01 | Generated on 2025-05-27 10:27:01

In bacterial BL, S_1-HFOH is obtained by the dissociation of the peroxide HFOOCH(OH)R [see Scheme 1(a)]. Our previous theoretical calculations suggested that this dissociation process takes place through charge transfer initialed luminous (CTIL) mechanism [35]. To better explore the ET mechanism, we calculated the potential energy curves (PECs) of S_0, S_1, second excited singlet (S_2), first excited triplet (T_1) and second excited triplet (T_2) states in the decomposition process of HFOOCH(OH)R. Along the PECs, the geometries at the S_0 state were obtained at the CAM-B3LYP/6-31+G** level [35] and the solvation effects of buried active sites of *VH*Luc were considered by using polarized continuum model (PCM) [36,37] with a dielectric of 4 [38,39]. Based on the previous theoretical calculations [35], in this study, the spin-flip time-dependent density functional theory (SF-TDDFT) method was used to calculate the PECs of S_0, S_1, S_2, T_1 and T_2 states in the decomposition process of HFOOCH(OH)R via the GAMESS US package [40]. The BHHLYP functional with 6-31G** basis set was applied in the SF-TDDFT calculations, this computational level showed good performances in the previous SF-TDDFT benchmark work [41], see the SI for details.

2.4 QM/MM calculations

In this paper, the vertical absorption wavelength (λ_A, nm) of ground state (S_0)-DLZ and the vertical emission wavelength (λ_F, nm) of S_1-DLZ in *PK*LumP were calculated by using the high-level QM/MM method. The DLZ was involved in the QM region, while the remaining atoms were involved in the MM region. An active space of 14-in-12 was used (see Figure S6) for S_0- and S_1-DLZ to perform complete active space self-consistent field (CASSCF) [42] and complete active space second-order perturbation theory (CASPT2) [43] calculations. The structures of S_0- and S_1-DLZ were optimized at the CASSCF/ANO-RCC-VDZP/MM level. The oscillator strength (f), λ_A and λ_F were calculated at the CASPT2/ANO-RCC-VDZP/MM level. As for calculating the λ_F of S_1-HFOH in *VH*Luc, the C-C single bond connecting with N_{10} was cut off in R′ group and an H link atom was added. The HFOH was involved in the QM region, while the remaining atoms were involved in the MM region. An activation space of 14-in-12 was used (see Figure S7) for HFOH and the calculation level was consistent with that for DLZ. For the MM region in QM/MM calculations, the side chains of residues and the water molecules within 5 Å of QM region were allowed to relax during the optimizations. To consider the effect of the protein fluctuation on the absorption and emission spectra [44,45], we selected five snapshots at 5, 5.5, 6, 6.5 and 7 ns in the production region from the MD trajectories, and used the geometry of these snapshots as the initial geometry of the QM/MM calculations to calculate λ_A and λ_F. The QM region employed CASPT2 method due to its well performance in the description of the properties of excited-state molecules [46]. The calculated λ_A and λ_F values at the other five different snapshots are similar (see Tables S1 and S2 in SI). The combination of Molcas [47] and Tinker [48] packages were used for the above QM/MM calculations. The electrostatic potential fitted (ESPF) method was used to achieve the electrostatic coupling between the QM and MM region [49].

2.5 Föster Resonance Energy Transfer (FRET) calculations

ET occurs between an energy donor at the excited state (D^*) and an energy acceptor at the ground state (A). In the system we studied, S_1-HFOH is the donor (D^*) and S_0-DLZ is the acceptor (A). The rate of FRET from a donor to an acceptor can be calculated by formula (1) [50-52]

$$k_{\mathrm{ET}} = (\hbar^2 c)^{-1} |V_{\mathrm{DA}}|^2 J \tag{1}$$

where $\hbar$ is the reduced Planck constant and c is the light speed. V_{DA} represents the electrostatic interaction between the initial state D^*A and the final state DA^*. Considering point dipole approximation and the influence of the solvent environment, V_{DA} can be expressed as:

$$\begin{aligned} |V_{\mathrm{DA}}|^2 &= \left| \frac{1}{4\pi\varepsilon_0 \eta^2 r^3} \left[(\vec{\mu}_{\mathrm{D}} \cdot \vec{\mu}_{\mathrm{A}}) - \frac{3}{r^2} (\vec{\mu}_{\mathrm{D}} \cdot \vec{r})(\vec{\mu}_{\mathrm{A}} \cdot \vec{r}) \right] \right|^2 \\ &= \frac{1}{(4\pi\varepsilon_0)^2} \frac{\kappa^2}{\eta^4 r^6} |\mu_{\mathrm{D}}|^2 |\mu_{\mathrm{A}}|^2 \end{aligned} \tag{2}$$

Here, $\vec{\mu}_{\mathrm{D(A)}}$ denotes the transition dipole moment (TDM) vector of donor (acceptor), while $\vec{r}$ represents the distance vector between them. ε_0 is the vacuum permittivity and η corresponds to the refractive index of the solvent environment, which is set to 1.33 (for water) in this study. The orientation factor, κ^2, which describes the relative orientation of the donor and acceptor TDMs, is given by formula (3).

$$\kappa^2 = (\cos\theta_{\mathrm{T}} - 3\cos\theta_{\mathrm{D}} \cos\theta_{\mathrm{A}})^2 \tag{3}$$

θ_{T} represents the angle between $\vec{\mu}_{\mathrm{D}}$ and $\vec{\mu}_{\mathrm{A}}$, while θ_{D} and θ_{A} denote the angle between $\vec{\mu}_{\mathrm{D}}$ and $\vec{r}$, and between $\vec{\mu}_{\mathrm{A}}$ and $\vec{r}$, respectively. J in formula (1) corresponds to the overlap integral of the donor's normalized emission spectrum [$F_{\mathrm{D}}(\tilde{\nu})$] and the acceptor's normalized absorption spectrum [$A_{\mathrm{A}}(\tilde{\nu})$]. The integral J is mathematically defined in formula (4). In the spectral overlap region, the emission energy of the donor matches the absorption energy of the acceptor, this resonance condition makes it possible for the occurrence of energy transfer process, where the total system transits from the initial state D^*A to the final state DA^*. The size of the overlap region is related to the broadening of spectrum, which is usually caused by the coupling between electronical states and vibrational states (vibronic coupling).

$$J = \int_0^\infty F_{\mathrm{D}}(\tilde{\nu}) A_{\mathrm{A}}(\tilde{\nu})\, d\tilde{\nu} \tag{4}$$

$F_{\mathrm{D}}(\tilde{\nu})$ and $A_{\mathrm{A}}(\tilde{\nu})$ can be obtained from the emission spectrum [$f_{\mathrm{D}}(\tilde{\nu})$] and absorption spectrum [$\varepsilon_{\mathrm{A}}(\tilde{\nu})$] by formula (5) and (6). $\tilde{\nu}$ is the wavenumber in cm^{-1}.

$$F_{\mathrm{D}}(\tilde{\nu}) = \frac{f_{\mathrm{D}}(\tilde{\nu})/\tilde{\nu}^3}{\int_0^\infty d(\tilde{\nu})\, f_{\mathrm{D}}(\tilde{\nu})/\tilde{\nu}^3} \tag{5}$$

$$A_{\mathrm{A}}(\tilde{\nu}) = \frac{\varepsilon_{\mathrm{A}}(\tilde{\nu})/\tilde{\nu}}{\int_0^\infty d(\tilde{\nu})\, \varepsilon_{\mathrm{A}}(\tilde{\nu})/\tilde{\nu}} \tag{6}$$

The values of $|\mu_{\mathrm{D}}|^2$ and $|\mu_{\mathrm{A}}|^2$ can be obtained from the QM/MM calculations. A detailed explanation of the formula derivations can be

DOI https://doi.org/10.4208/cicc.2025.71.01 | Generated on 2025-05-27 10:27:01

found in the Supporting Information (SI). Based on the concepts introduced above, the calculation process is presented in Scheme 2.

2.6 The calculation of spectrum, radiative and non-radiative rates

The simulations of the absorption spectrum (acceptor), the emission spectrum (donor), and the calculations of the radiative (k_R) and non-radiative (k_{NR}) decay rates of donor and acceptor at 300K were performed by using the thermal vibration correlation function (TVCF) formalism in the MOMAP package [53-56], see SI for details. The quantum yield of the radiative process was calculated by formula (7).

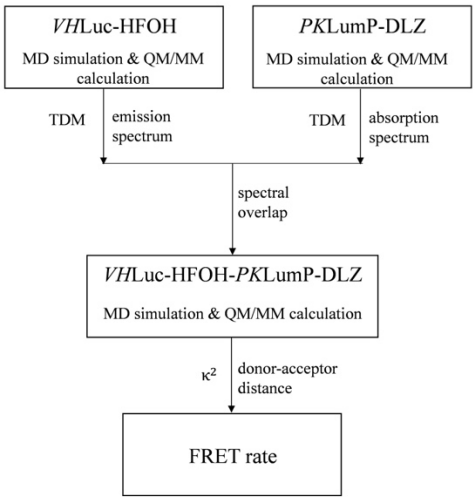

Scheme 2. Workflow of the FRET rate calculation approaches.

$$\Phi = \frac{k_R}{k_R + k_{NR}} \quad (7)$$

In TVCF calculations, it is crucial to determine the geometries and vibrational frequencies of S_0- and S_1-HFOH in *VH*Luc, as well as those of S_0- and S_1-DLZ in *PK*LumP. Additionally, the TDMs, adiabatic energies and non-adiabatic couplings (NACs) between the S_0 and S_1 states are also required. In this study, the adiabatic energies of HFOH and DLZ between S_0 and S_1 states, along with their TDMs, were computed at the CASPT2//CASSCF/ANO-RCC-VDZP/MM level. Meanwhile, the vibrational frequencies of HFOH and DLZ at the S_0 and S_1 states, as well as the NACs between them, were determined using the ONIOM methodology at the (TD) CAM-B3LYP/6-31G**/MM level, implemented in the Gaussian 16 package.

3. Results and discussion

3.1 Analysis of the *VH*Luc-*PK*LumP complex interface

In order to investigate the mechanism of ET between HFOH and DLZ, we first analyzed the structure of *VH*Luc-*PK*LumP. Before protein-protein docking, the substrate DLZ of *PK*LumP, is on the surface of the protein, while the substrate HFOH of *VH*Luc is on the β-barrel of the α subunit (Figure S8). The structure of *VH*Luc-*PK*LumP is shown in Figure S9(a). The Fpocket program [57, 58] was employed to detect the cavity of *VH*Luc-*PK*LumP and the result revealed that DLZ and HFOH occupy the same cavity as shown in Figure S9(b). This provides conditions for the subsequent ET process. Subsequently, the properties of the interface of *VH*Luc-*PK*LumP were analyzed on the PDBePISA server [59]. The analysis results shown in Figure 1 indicate that hydrogen bonds could be formed between Glu15, Glu210, His285, Asp287, Arg291, Asp293, Tyr294 of *VH*Luc and Met1, Thr21, Val41, Gln65, Arg86, Lys103, Asp127, Thr182 of *PK*LumP to assist the *VH*Luc-*PK*LumP stabilization. More detailed information for the formation of hydrogen bonds is shown in Table S3. The buried surface area (BSA) of *VH*Luc-*PK*LumP was calculated to be 2,606 Å^2 which is large enough for the protein-protein complex [60]. The interfacing residues are shown in Table S4. The surface electrostatic potential of *PK*LumP and *VH*Luc were calculated by PDB2PQR and evaluated in Adaptive Poisson-Boltzmann Solver (APBS) [61]. The calculation results are shown in Figure S10. The results indicate that the interface have charge complementarity between Glu175, Lys259, Lys283, Asp287, Asp293 in *VH*Luc and Met1, Glu34, Ser35, Val36, Gln65, Leu93, Lys103 in *PK*LumP. Based on the discussion above, the formation of hydrogen bonds at the interface and the presence of electrostatic interactions can improve the stability of *VH*Luc-*PK*LumP.

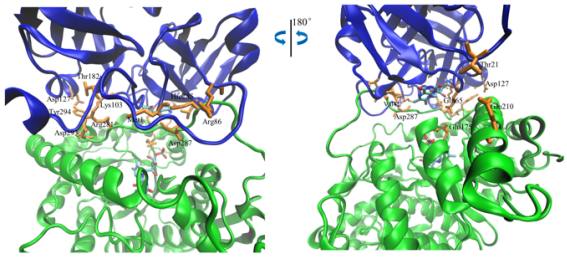

Figure 1. Views of amino acid residues that form hydrogen bonds between *VH*Luc and *PK*LumP in the *VH*Luc-*PK*LumP interface analyzed by PDBePISA [59]. The blue-colored protein represents *PK*LumP, while the green-colored protein represents *VH*Luc.

3.2 The mechanism of energy transfer from HFOH to DLZ in *VH*Luc-*PK*LumP

Usually, the nonradiative ET can happen through Dexter energy transfer (DET) or FRET [62,63]. For FRET, ET from the donor to the acceptor is mediated by Coulombic interactions [62,64], whereas DET relies on orbital overlap and electron exchange [63, 65]. Generally, the effective distance for orbital overlap and electron exchange between the donor and acceptor is limited to approximately 10 Å, while Coulombic interactions can extend up to 100 Å. Therefore, the FRET mechanism is mainly considered when donor and acceptor are far apart (10-100 Å), while the DET mechanism is considered only when donor and acceptor are close enough (< 10 Å) [66,67]. As illustrated in Figure S11, our 100 ns MD simulation results indicate that the donor-acceptor distance falls within the range of 17–23 Å. This means that the ET process from HFOH to DLZ follows the FRET mechanism, which is consistent with Lee's opinion [20].

Bioluminophore comes from the decomposition of peroxide in BL, such as firefly [68,69], jellyfish [70], firefly squid [71],

DOI https://doi.org/10.4208/cicc.2025.71.01 | Generated on 2025-05-27 10:27:01

fugus, [72] bacteria [35] and so on. In bacterial BL, HFOH is generated by the decomposition of HFOOCH(OH)R [see Scheme1(a)]. We calculated the decomposition process of HFOOCH(OH)R and the calculation results are shown in Figure S12. From Figure S12, the entire reaction can release energy of about 107.5 kcal/mol (270 nm in wavelength), which means that the energy released is enough to excite HFOH. However, the product HFOH could be in different excited states. In order to determine the ET process from which state of HFOH to S_0-DLZ via FRET mechanism, we calculated the PECs of S_0, S_1, S_2, T_1 and T_2 states in decomposition process of HFOOCH(OH)R (see Figure S13). Because of the large energy gap between S_0- and S_2-PECs (the minimum energy gap >20 kcal/mol), only S_1-, T_1-, and T_2-HFOH will be generated. Subsequently, to explore the possibility of ET from T_2- and T_1-HFOH in *VH*Luc to S_0-DLZ in *PK*LumP by FRET mechanism [T_2/T_1 (HFOH) + S_0 (DLZ) → S_0 (HFOH) + S_1 (DLZ)], the energy gaps between T_2-HFOH and S_0-HFOH, as well as T_1-HFOH and S_0-HFOH, were calculated. The calculated energy gap of 77.4 kcal/mol (370 nm) between the T_2- and S_0-HFOH in *VH*Luc is enough to excite DLZ in *PK*LumP from the S_0 to the S_1 state (68.2 kcal/mol, 420 nm) [73]. However, the energy gap between the T_1- and S_0-HFOH in *VH*Luc is 47.0 kcal/mol (609 nm), which is lower than the absorption energy of S_0-DLZ in *PK*LumP. The spin-orbital coupling (SOC) constant was calculated between the T_2- and S_0-HFOH, as well as the T_2- and S_1-HFOH in *VH*Luc to be 0.17 and 0.54 cm^{-1}, respectively. The SOC constant between the T_1- and S_0-HFOH, as well as the T_1- and S_1-HFOH in *VH*Luc to be 0.73 and 0.09 cm^{-1}. The obtained SOC value indicates that the intersystem crossing (ISC) from the T_2- and T_1-HFOH to the S_0-HFOH in *VH*Luc is unlikely to occur. Therefore, the possibility of ET from the T_2- and T_1-HFOH in *VH*Luc to the S_0-DLZ in *PK*LumP by FRET mechanism can be ruled out.

Currently, we only need to consider ET from S_1-HFOH in *VH*Luc to S_0-DLZ in *PK*LumP by FRET mechanism [S_1 (HFOH) + S_0 (DLZ) → S_0 (HFOH) + S_1 (DLZ)]. The rate of FRET (k_{ET}) is determined using formula (1). To obtain the necessary parameters for this calculation, the overlap integral between the emission spectrum of S_1-HFOH in *VH*Luc and the absorption spectrum of S_0-DLZ in *PK*LumP must be calculated. After calculating the overlap integral, k_{ET} needs to be determined in *VH*Luc-*PK*LumP. One, a snapshot was randomly selected from the equilibrated region of the MD simulation, and its geometry was used as the initial geometry for QM/MM optimization. The CASSCF/ANO-RCC-VDZP/MM optimized S_0-DLZ geometry in *PK*LumP and the S_1-HFOH geometry in *VH*Luc as well as the hydrogen bonding networks around them are drawn in Figure 2. Under the influence of these hydrogen-bonding interactions, both S_1-HFOH and S_0-DLZ maintain a stable planar configuration. Two, the values of λ_F, λ_A and TDM for S_1-HFOH and S_0-DLZ were computed at the CASPT2/ANO-RCC-VDZP/MM level. The results of these calculations are summarized in Table S5. By comparing the data from Tables S1, S2, and S5, we found that the λ_F and λ_A values obtained from the randomly selected snapshot closely match the average values derived from five different snapshots, confirming the reliability of our approach.

The transitions of DLZ and HFOH between the S_0 and S_1 states both belong to π-π^* type (see Figures S6 and S7 for orbitals), which are consistent with their large TDMs. Three, based on the CASPT2 calculated results (energies and TDMs).

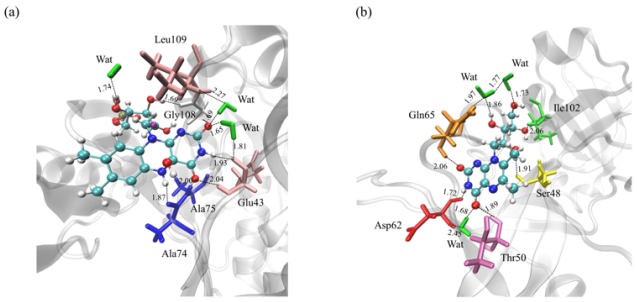

Figure 2. Optimized geometries and hydrogen bonding networks of S_1-HFOH in *VH*Luc (a) and S_0-DLZ in *PK*LumP (b) at the CASSCF/ANO-RCC-VDZP/MM level. The purple atom in (a) is the H link atom. The unit of hydrogen bond length is Å.

and the DFT/TDDFT calculated vibrational frequencies at the S_0 and S_1 states, the absorption spectrum of S_0-DLZ and the emission spectrum of S_1-HFOH and were simulated by using the TVCF formalism in the MOMAP package. It should be noted that we both considered the electronic states and the vibrational states in the simulation of spectra. The simulation results are shown in Figure 3, which agrees very well with the experimental results, see the caption of Figure 3 for details. At last, the calculated spectral overlap (yellow region in Figure 3) integral J by formula (4) is 2.49×10^{-5} cm.

In the equilibrated region of the 100 ns MD trajectory of *VH*Luc-*PK*LumP, we selected an representative equilibrated structure and performed geometry optimization of the QM region (HFOH and DLZ) on the S_1 state at the TD CAM-B3LYP/6-31G**/MM level. The calculation process is shown in Figure 4. In Figure 4, the red arrows represent the TDMs ($\vec{\mu}$) of the donor and acceptor while the blue arrow denotes the distance vector $\vec{r}$ connecting the chromophore centers of mass of the donor and acceptor (yellow dots in Figure 4). Based on this structural analysis, the donor-acceptor distance r was estimated to be 19.8 Å. Additionally, $\cos\theta_T$, $\cos\theta_A$ and $\cos\theta_D$ were calculated to be 0.235, -0.424 and -0.699, as shown in Figure 4 (see Table S6 for calculation details). Therefore, the orientation factor κ^2 was 0.43

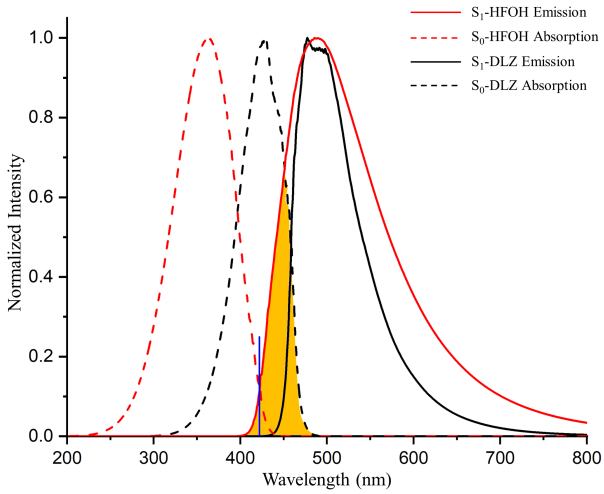

Figure 3. Simulated absorption spectrum of S_0-HFOH (peak at 363 nm) and emission spectrum of S_1-HFOH (**peak at 486 nm, exp: 485 nm** [74]) in *VH*Luc. Simulated absorption spectrum of S_0-DLZ (**peak at 427 nm, exp: 420 nm** [73]) and emission

DOI https://doi.org/10.4208/cicc.2025.71.01 | Generated on 2025-05-27 10:27:01

spectrum of S_1-DLZ (**peak at 477 nm, exp: 475 nm**[9]) in *PK*LumP. The yellow region represents the spectral overlap. The blue line represents the 0-0 transition (about 423 nm) between S_0- and S_1-HFOH.

by using formula (3). Based on the previously obtained results, $|V_{DA}|^2$ was calculated as 1.34×10^{-44} $kg^2m^4s^{-4}$. Finally, using formula (1), k_{ET} was calculated to be 1.01×10^9 s^{-1}. To further validate these results, we selected three additional snapshots from the MD trajectory at 60, 70, and 80 ns as initial geometries for QM/MM calculations and computed the corresponding FRET rates. As shown in Table S7, all calculated FRET rates are ~10^9 s^{-1}, demonstrating the consistency of our results.

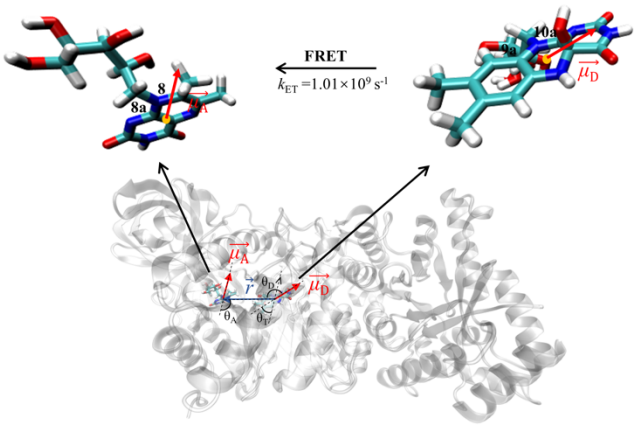

Figure 4. Optimized geometries of HFOH and DLZ complex at the S_1 state computed at the TD CAM-B3LYP/6-31G**/MM level. For the enlarged part on the left, the red arrow is the TDM of DLZ ($\vec{\mu}_A$) and the yellow dot indicates the center of mass of DLZ chromophore. For the enlarged part on the right, the red arrow is the TDM of HFOH ($\vec{\mu}_D$) and the yellow dot indicates the center of mass of HFOH chromophore. The center of mass of (yellow dots shown in figure) donor and acceptor represent the two ends of the distance vector $\vec{r}$ (blue arrow). The direction of the TDM of DLZ is along the direction from C_{8a} to C_8. The direction of the TDM of HFOH is along the direction from C_{9a} to C_{10a}. θ_T, θ_A and θ_D represent the angles between the three vectors $\vec{\mu}_A$, $\vec{\mu}_D$ and $\vec{r}$.

We also computed the fluorescence rates (k_F) and internal conversion rates (k_{IC}) of S_1-HFOH in *VH*Luc and S_1-DLZ in *PK*LumP, from the S_1 state to the S_0 state, using the TVCF formalism via the MOMAP package. In the studied system, fluorescence is the exclusive pathway for radiative decay, which means k_F is equivalent to k_R. Due to the small SOC values between the S_1 and T_1 states of HFOH (0.09 cm^{-1}) and DLZ (0.14 cm^{-1}), computed at the CASPT2/ANO-RCC-VDZP//CASSCF/ANO-RCC-VDZP/MM level, the ISC process between the S_1 and T_1 states can be neglected. Consequently, we consider k_{IC} to be approximately equal to k_{NR}. The fluorescence quantum yield (Φ_F) was calculated using formula (7). The computational results are summarized in Table 1. The k_R and k_{NR} of S_1-HFOH are 6.14×10^7 and 1.12×10^8 s^{-1}, respectively. After the addition of *PK*LumP to the BL system of *VH*Luc, the *VH*luc-*PK*LumP complex is formed accompanied by the FRET process from S_1-HFOH to S_0-DLZ. The calculated FRET rate to be 1.01×10^9 s^{-1}, which is much larger than the k_R and k_{NR} of S_1-HFOH. This indicates that the FRET process from S_1-HFOH to S_0-DLZ occurs with high efficiency in the *VH*Luc-*PK*LumP complex. After the efficient FRET process, S_0-DLZ is excited to S_1-DLZ. As shown in Table 1, the calculated Φ_F of S_1-DLZ is about 1.9 times that of S_1-HFOH, which well explain the observed 2.1-fold enhancement in BL intensity.

Usually, when FRET occurs between organic molecules, the maximum emission wavelength is red-shifted. The blue-shifted ET process has been found in metal nanoparticles-semiconductor and metal nanoparticles-organic molecule systems [75-77]. Researchers believed that this phenomenon follows the plasmon-induced resonance energy transfer (PIRET) mechanism [76, 78]. The main reason is that the metal nanoparticles have small Stokes shift, leading to the good spectral overlap between donor and acceptor. In the *PP* BL process, the experimentally determined maximum emission wavelength of S_1-DLZ (475 nm) is shorter than the maximum emission wavelength of S_1-HFOH (485 nm). This is well verified by the present calculations (S_1-HFOH: 486 nm, S_1-DLZ: 477 nm in Figure 3) as experiment. For the above unusual blue-shifted FRET process occurring between organic molecules, we can explain this phenomenon with the similar idea as PIRET mechanism. First, there is a large overlap between the absorption spectrum of S_0-DLZ and emission spectrum of S_1-HFOH, which ensures the efficient FRET from the donor to the acceptor. From Figure 3, we can see that the broad emission spectrum of S_1-HFOH, which is mostly caused by the strong vibronic coupling of HFOH molecule. The energies of vibronic transitions of S1-HFOH in the spectral overlap region are higher than the emission peak of S_1-DLZ (477 nm) as shown in Figure 3, which guarantees S_1-DLZ still has enough energy to emit light after FRET. These high-energy vibronic transitions can resonate with the vibronic transitions of S_0-DLZ (spectral overlap region in Figure 3), resulting in the ET from S_1-HFOH to S_0-DLZ The whole ET process still follows the principles of energy conservation. Due to the small Stokes shift (50 nm in our calculation) of DLZ, the maximum emission wavelength of S_1-DLZ is blue-shifted compared with the maximum emission wavelength of S_1-HFOH. The experimentally determined Stokes shift of DLZ is 82 nm in water [14] and 55 nm in *PP*LumP [18, 73]. The smaller Stokes shift in *PP*LumP than in water is due to the formation of H-bond network between DLZ and residues, which limits structural changes of DLZ and increases its rigidity.

Table 1. The calculated radiative rate (k_R), non-radiative rate (k_{NR}) and fluorescence quantum yield (Φ_F) of S_1-HFOH in *VH*Luc and S_1-DLZ in *PK*LumP.

	S_1-HFOH in *VH*Luc	S_1-DLZ in *PK*LumP
k_R (s^{-1})	6.14×10^7	3.30×10^7
k_{NR} (s^{-1})	1.12×10^8	1.60×10^7
Φ_F	0.35 (0.33[a])	0.67 (0.54[b])

[a]. The fluorescence quantum yield of luciferase from *Vibrio Harveyi* at 2 ℃ [79]. [b]. The fluorescence quantum yield of LumP from *Photobacterium leiognathi* at 20 ℃ [80].

DOI https://doi.org/10.4208/cicc.2025.71.01 | Generated on 2025-05-27 10:27:01

Based on the above discussion, the calculation results demonstrate that, after the ET in *VH*Luc-*PK*LumP, S_0-DLZ is excited to S_1-DLZ and subsequently emits BL. Our protein-protein docking results predicted a favorable interaction between *VH*Luc and *PK*LumP. The QM/MM calculations confirmed that the electronic structures of HFOH and DLZ are well-suited for FRET, with significant overlap between the emission spectrum of S_1-HFOH and the absorption spectrum of S_0-DLZ. The experimentally estimated k_{ET} is in the range of 4×10^8 to 10^9 s^{-1} [81]. The ET rate calculated from our docking model falls within the estimated range. Moreover, since the donor and acceptor are within proteins, their relative orientation is constrained and cannot be assumed to be random. Therefore, the commonly used $\kappa^2 = 2/3$ value for random orientation cannot be applied in this case. Instead, we calculated a specific κ^2 value based on our actual system, which represents an improvement over traditional experimental methods that rely on the average κ^2 value.

4. Conclusion

Most of the known bioluminescent bacteria species emits BL around 490 nm, but *PP* emits 475 nm BL and much brighter. Besides the regular bioluminescent system of HFOH-*PP*Luc, *PP* has an extra bioluminescent system, DLZ-*PP*LumP. The 475 nm wavelength light is emitted by the latter system after an ET from the former system. We thoroughly investigated the blue-shifted ET mechanism. *PP*Luc and *PP*LumP were reasonably replaced by *VH*Luc and *PK*LumP, respectively. We obtained *VH*Luc-*PK*LumP complex structure by protein-protein docking indicating that a FRET process occurs from S_1-HFOH to S_0-DLZ. The FRET rate was calculated to be ~10^9 s^{-1} through the MD simulations and QM/MM calculations, which is faster than the S_1-HFOH radiative rate (~10^7 s^{-1}) and non-radiative rate (~10^8 s^{-1}). The fast FRET rate indicates that the FRET from S_1-HFOH to S_0-DLZ in *VH*Luc-*PK*LumP occurs efficiently. The small Stokes shift of DLZ as well as the strong vibronic coupling of HFOH allow the blue-shifted FRET process. The calculated Φ_F of S_1-DLZ in *PK*LumP is 1.9-fold than that of S_1-HFOH in *VH*Luc, which explains the 2.1-fold enhancement in BL intensity of *PP*. The understanding on the ET in the *PP* system not only did it help us deepen our understanding of the entire bacterial BL process, but also helps to understand other bioluminescent systems and provides new insights into BRET. The understanding of the ET mechanism in the *PP* system has not only enhanced our comprehension of the entire bacterial BL process but also contributes significantly to the broader understanding of various bioluminescent systems. Moreover, it provides valuable contributions to the development of BRET techniques, thereby providing new insights for applications in molecular biology, diagnostics, and real-time cellular imaging.

Supporting Information

The following supporting information can be downloaded at: https://global-sci.com/storage/self-storage/104208cicc20257101.pdf.

Acknowledgments

This work was supported by grants from the National Natural Science Foundation of China (Nos. 22373010 and 21973005), the Beijing Natural Science Foundation (No. 2244074), the Guangdong Basic and Applied Basic Research Foundation (No. 2025A1515012183) and the start-up funding (No. 312200502511) from Beijing Normal University at Zhuhai. Computing resources were provided by the Interdisciplinary Intelligence SuperComputer Center of Beijing Normal University at Zhuhai. We gratefully acknowledge HZWTECH for providing computation facilities.

References

[1] P.J. Herring, Systematic distribution of bioluminescence in living organisms. *J. Biolumin. Chemilumin.*, **1** (1987), 147-163.

[2] J.-B. Li, Q. Wang, H.-W. Liu, L. Yuan, X.-B. Zhang, A bioluminescent probe for imaging endogenous hydrogen polysulfides in live cells and a murine model of bacterial infection. *Chem. Commun.*, **55** (2019), 4487-4490.

[3] S. Sharifian, A. Homaei, R. Hemmati, R. B. Luwor, K. Khajeh, The emerging use of bioluminescence in medical research. *Biomed. Pharmacother.*, **101** (2018), 74-86.

[4] T. Axelrod, E. Eltzov, R.S. Marks, Bioluminescent bioreporter pad biosensor for monitoring water toxicity. *Talanta*, **149** (2016), 290-297.

[5] S. Schramm, M.B. Al-Handawi, D.P. Karothu, A. Kurlevskaya, P. Commins, Y. Mitani, C. Wu, Y. Ohmiya, P. Naumov, Mechanically assisted bioluminescence with natural luciferase. *Angew. Chem. Int. Ed.*, **59** (2020), 16485-16489.

[6] M. van Oosten, T. Schäfer, J.A.C. Gazendam, K. Ohlsen, E. Tsompanidou, M.C. de Goffau, H.J.M. Harmsen, L.M.A. Crane, E. Lim, K.P. Francis, L. Cheung, M. Olive, V. Ntziachristos, J.M. van Dijl, G.M. van Dam, Real-time in vivo imaging of invasive- and biomaterial-associated bacterial infections using fluorescently labelled vancomycin. *Nat. Commun.*, **4** (2013), 2584.

[7] J.W. Hastings, C.J. Potrikusv, S.C. Gupta, M. Kurfürst, J.C. Makemson, Biochemistry and physiology of bioluminescent bacteria, in: A.H. Rose, D.W. Tempest (Eds.) Adv. Microb. Physiol., Academic Press, London, 1985, pp. 235-291.

[8] E. Brodl, A. Winkler, P. Macheroux, Molecular mechanisms of bacterial bioluminescence. *Comput. Struct. Biotechnol. J.*, **16** (2018), 551-564.

[9] J. Lee, F. Müller, A.J.W.G. Visser, The sensitized bioluminescence mechanism of bacterial luciferase. *Photochem. Photobiol.*, **95** (2019), 679-704.

[10] J. Lee, Bioluminescence, The Nature of The Light., University of Georgia Libraries, Athens, GA, 2017.

[11] J. Lee, Matheson, Myuller, O'Kane, Vervoort, A. Visser, Chemistry and Biochemistry of Flavins and Flavoenzymes., CRC, Orlando, 1991.

[12] P. Macheroux, S. Ghisla, J.W. Hastings, Spectral detection of an intermediate preceding the excited state in the bacterial luciferase reaction. *Biochemistry*, **32** (1993), 14183-14186.

[13] Y. Luo, Y.-J. Liu, Bioluminophore and flavin mononucleotide fluorescence quenching of bacterial bioluminescence—a theoretical study. *Chem. Eur. J.*, **22** (2016), 16243-16249.

[14] P. Koka, J. Lee, Separation and structure of the prosthetic group of the blue fluorescence protein from the bioluminescent

bacterium Photobacterium phosphoreum. *Proc. Natl. Acad. Sci.*, **76** (1979), 3068-3072.

[15] D.J. O'Kane, B. Woodward, J. Lee, D.C. Prasher, Borrowed proteins in bacterial bioluminescence. *Proc. Natl. Acad. Sci.*, **88** (1991), 1100-1104.

[16] D.J. O'Kane, V.A. Karle, J. Lee, Purification of lumazine proteins from Photobacterium leiognathi and Photobacterium phosphoreum: bioluminescence properties. *Biochemistry*, **24** (1985), 1461-1467.

[17] E.D. Small, P. Koka, J. Lee, Lumazine protein from the bioluminescent bacterium Photobacterium phosphoreum: purification and characterization. *J. Biol. Chem.*, **255** (1980), 8804-8810.

[18] R. Gast, J. Lee, Isolation of the in vivo emitter in bacterial bioluminescence. *Proc. Natl. Acad. Sci.*, **75** (1978), 833-837.

[19] S.C. Daubner, A.M. Astorga, G.B. Leisman, T.O. Baldwin, Yellow light emission of Vibrio fischeri strain Y-1: purification and characterization of the energy-accepting yellow fluorescent protein. *Proc. Natl. Acad. Sci.*, **84** (1987), 8912-8916.

[20] J. Lee, Fluorescent antenna proteins from the bioluminescent bacteria. *Microsc. Microanal.*, **4** (1998), 1002-1003.

[21] K.J. Fujimoto, T. Seki, T. Minoda, T. Yanai, Spectral tuning and excitation-energy transfer by unique carotenoids in diatom light-harvesting antenna. *J. Am. Chem. Soc.*, **146** (2024), 3984-3991.

[22] Dragulescu-Andrasi, C.T. Chan, A. De, T.F. Massoud, S.S. Gambhir, Bioluminescence resonance energy transfer (BRET) imaging of protein–protein interactions within deep tissues of living subjects. *Proc. Natl. Acad. Sci.,* **108** (2011), 12060-12065.

[23] Y. Sato, S. Shimizu, A. Ohtaki, K. Noguchi, H. Miyatake, N. Dohmae, S. Sasaki, M. Odaka, M. Yohda, Crystal structures of the lumazine protein from Photobacterium kishitanii in complexes with the authentic chromophore, 6,7-dimethyl- 8-(1'-D-ribityl) lumazine, and its analogues, riboflavin and flavin mononucleotide, at high resolution. *J. Bacteriol.*, **192** (2010), 127-133.

[24] Z.T. Campbell, A. Weichsel, W.R. Montfort, T.O. Baldwin, Crystal structure of the bacterial luciferase/flavin complex provides insight into the function of the beta subunit. *Biochemistry*, **48** (2009), 6085-6094.

[25] Waterhouse, M. Bertoni, S. Bienert, G. Studer, G. Tauriello, R. Gumienny, F.T. Heer, T.A P. de Beer, C. Rempfer, L. Bordoli, R. Lepore, T. Schwede, SWISS-MODEL: homology modelling of protein structures and complexes. *Nucleic Acids Res.*, **46** (2018), W296-W303.

[26] S. Bienert, A. Waterhouse, G. Tauriello, G. Studer, L. Bordoli, T. Schwede, The SWISS-MODEL repository—new features and functionality. *Nucleic Acids Res.*, **45** (2017), D313-D319.

[27] N. Guex, M.C. Peitsch, T. Schwede, Automated comparative protein structure modeling with SWISS-MODEL and Swiss-PdbViewer: a historical perspective. *Electrophoresis*, **30** (2009), S162-S173.

[28] J. Lee, D.J. O'Kane, B.G. Gibson, Bioluminescence spectral and fluorescence dynamics study of the interaction of lumazine protein with the intermediates of bacterial luciferase bioluminescence. *Biochemistry.*, **28** (1989), 4263-4271.

[29] J. Lee, Sensitization by lumazine proteins of the bioluminescence emission from the reaction of bacterial luciferases. *Photochem. Photobiol.*, **36** (1982), 689-697.

[30] Fiser, R.K.G. Do, A. Šali, Modeling of loops in protein structures. Protein Sci., 9 (2000), 1753-1773.

[31] Fiser, A. Sali, ModLoop: automated modeling of loops in protein structures. Bioinformatics, **19** (2003), 2500-2501.

[32] D. Schneidman-Duhovny, Y. Inbar, R. Nussinov, H.J. Wolfson, PatchDock and SymmDock: servers for rigid and symmetric docking. *Nucleic Acids Res.*, **33** (2005), W363-W367.

[33] N. Andrusier, R. Nussinov, H.J. Wolfson, FireDock: fast interaction refinement in molecular docking. *Proteins*, **69** (2007), 139-159.

[34] D. Case, R. Betz, D.S. Cerutti, T. Cheatham, T. Darden, R. Duke, T.J. Giese, H. Gohlke, A. Götz, N. Homeyer, S. Izadi, P. Janowski, J. Kaus, A. Kovalenko, T.-S. Lee, S. LeGrand, P. Li, C. Lin, T. Luchko, P. Kollman, Amber 16., University of California, San Francisco, 2016.

[35] S. Pi, Y. Luo, Y.-J. Liu, Thorough understanding of bioluminophore production in bacterial bioluminescence. *J. Phys. Chem. A*, **126** (2022), 6604-6616.

[36] J. Tomasi, B. Mennucci, R. Cammi, Quantum mechanical continuum solvation models. *Chem. Rev.*, **105** (2005), 2999-3094.

[37] S. Miertuš, E. Scrocco, J. Tomasi, Electrostatic interaction of a solute with a continuum: a direct utilizaion of ab initio molecular potentials for the prevision of solvent effects. *Chem. Phys.*, **55** (1981), 117-129.

[38] M.K. Gilson, B.H. Honig, The dielectric constant of a folded protein. *Biopolymers*, **25** (1986), 2097-2119.

[39] J.W. Pitera, M. Falta, W.F. van Gunsteren, Dielectric properties of proteins from simulation: the effects of solvent, ligands, pH, and temperature. *Biophys. J.*, **80** (2001), 2546-2555.

[40] M.W. Schmidt, K.K. Baldridge, J.A. Boatz, S.T. Elbert, M.S. Gordon, J.H. Jensen, S. Koseki, N. Matsunaga, K.A. Nguyen, S. Su, T.L. Windus, M. Dupuis, J.A. Montgomery Jr, General atomic and molecular electronic structure system. *J. Comput. Chem.*, **14** (1993), 1347-1363.

[41] S.V. Levchenko, A.I. Krylov, Equation-of-motion spin-flip coupled-cluster model with single and double substitutions: theory and application to cyclobutadiene. *J. Chem. Phys.*, **120** (2003), 175-185.

[42] B.O. Roos, P.R. Taylor, P.E.M. Sigbahn, A complete active space SCF method (CASSCF) using a density matrix formulated super-CI approach. *Chem. Phys.*, **48** (1980), 157-173.

[43] K. Andersson, P.Å. Malmqvist, B.O. Roos, Second-order perturbation theory with a complete active space self-consistent field reference function. *J. Chem. Phys.*, **96** (1992), 1218-1226.

[44] W. Arbelo-González, R. Crespo-Otero, M. Barbatti, Steady and time-resolved photoelectron spectra based on nuclear ensembles. *J. Chem. Theory Comput.*, **12** (2016), 5037-5049.

[45] Petrone, J. Cerezo, F.J.A. Ferrer, G. Donati, R. Improta, N. Rega, F. Santoro, Absorption and emission spectral shapes of a prototype dye in water by combining classical/dynamical and quantum/static approaches. *J. Phys. Chem. A.,* 119 (2015), 5426-5438.

DOI https://doi.org/10.4208/cicc.2025.71.01 | Generated on 2025-05-27 10:27:01

[46] Y.-J. Liu, Understanding the complete bioluminescence cycle from a multiscale computational perspective: a review. *J. Photochem. Photobiol., C*, **52** (2022), 100537.

[47] F. Aquilante, J. Autschbach, R.K. Carlson, L.F. Chibotaru, M.G. Delcey, L. De Vico, I. Fdez. Galván, N. Ferré, L.M. Frutos, L. Gagliardi, M. Garavelli, A. Giussani, C.E. Hoyer, G. Li Manni, H. Lischka, D. Ma, P.Å. Malmqvist, T. Müller, A. Nenov, M. Olivucci, T.B. Pedersen, D. Peng, F. Plasser, B. Pritchard, M. Reiher, I. Rivalta, I. Schapiro, J. Segarra-Martí, M. Stenrup, D.G. Truhlar, L. Ungur, A. Valentini, S. Vancoillie, V. Veryazov, V.P. Vysotskiy, O. Weingart, F. Zapata, R. Lindh, Molcas 8: new capabilities for multiconfigurational quantum chemical calculations across the periodic table. *J. Comput. Chem.*, **37** (2016), 506-541.

[48] J.A. Rackers, Z. Wang, C. Lu, M.L. Laury, L. Lagardere, M.J. Schnieders, J.P. Piquemal, P. Ren, J.W. Ponder, Tinker 8: software tools for molecular design. *J. Chem. Theory Comput.*, **14** (2018), 5273-5289.

[49] N. Ferré, J.G. Ángyán, Approximate electrostatic interaction operator for QM/MM calculations. *Chem. Phys. Lett.*, **356** (2002), 331-339.

[50] M. Anzola, C. Sissa, A. Painelli, A.A. Hassanali, L. Grisanti, Understanding forster energy transfer through the lens of molecular dynamics. *J. Chem. Theory Comput.*, **16** (2020), 7281-7288.

[51] R. Jacobi, D. Hernández-Castillo, N. Sinambela, J. Bösking, A. Pannwitz, L. González, Computation of Förster resonance energy transfer in lipid bilayer membranes. *J. Phys. Chem. A*, **126** (2022), 8070-8081.

[52] S. Petry, J.C. Tremblay, J.P. Götze, Impact of structure, coupling scheme, and state of interest on the energy transfer in CP29. *J. Phys. Chem. B*, **127** (2023), 7207-7219.

[53] Y. Niu, W. Li, Q. Peng, H. Geng, Y. Yi, L. Wang, G. Nan, D. Wang, Z.J.M.P. Shuai, Molecular materials property prediction package (MOMAP) 1.0: a software package for predicting the luminescent properties and mobility of organic functional materials. *Mol. Phys.*, **116** (2018), 1078-1090.

[54] Z. Shuai, Thermal vibration correlation function formalism for molecular excited state decay rates. *Chin. J. Chem.*, **38** (2020), 1223-1232.

[55] Z. Shuai, Q. Peng, Excited states structure and processes: understanding organic light-emitting diodes at the molecular level. *Phys. Rep.*, **537** (2014), 123-156.

[56] Z. Shuai, Q. Peng, Organic light-emitting diodes: theoretical understanding of highly efficient materials and development of computational methodology. *Natl. Sci. Rev.*, **4** (2017), 224-239.

[57] P. Schmidtke, V. Le Guilloux, J. Maupetit, P. Tufféry, Fpocket: online tools for protein ensemble pocket detection and tracking. *Nucleic Acids Res.*, **38** (2010), W582-W589.

[58] V. Le Guilloux, P. Schmidtke, P. Tuffery, Fpocket: an open source platform for ligand pocket detection. *BMC Bioinf.*, **10** (2009), 168.

[59] E. Krissinel, K. Henrick, Inference of macromolecular assemblies from crystalline state. *J. Mol. Biol.*, **372** (2007), 774-797.

[60] L.L. Conte, C. Chothia, J. Janin, The atomic structure of protein-protein recognition sites11edited by A. R. Fersht. *J. Mol. Biol.*, **285** (1999), 2177-2198.

[61] E. Jurrus, D. Engel, K. Star, K. Monson, J. Brandi, L.E. Felberg, D.H. Brookes, L. Wilson, J. Chen, K. Liles, M. Chun, P. Li, D.W. Gohara, T. Dolinsky, R. Konecny, D.R. Koes, J.E. Nielsen, T. Head-Gordon, W. Geng, R. Krasny, G.-W. Wei, M.J. Holst, J.A. McCammon, N.A. Baker, Improvements to the APBS biomolecular solvation software suite. *Protein Sci.*, **27** (2018), 112-128.

[62] T. Förster, 10th spiers memorial lecture: transfer mechanisms of electronic excitation. *Discuss. Faraday Soc.*, **27** (1959), 7-17.

[63] D.L. Dexter, A theory of sensitized luminescence in solids. *J. Chem. Phys.*, **21** (1953), 836-850.

[64] Z.-Q. You, C.-P. Hsu, Theory and calculation for the electronic coupling in excitation energy transfer. *Int. J. Quantum Chem*, **114** (2014), 102-115.

[65] S. Bai, P. Zhang, D.N. Beratan, Predicting Dexter energy transfer interactions from molecular orbital overlaps. *J. Phys. Chem. C*, **124** (2020), 18956-18960.

[66] J. Han, X. Chen, L. Shen, Y. Chen, W. Fang, H. Wang, Energy transfer tunes phosphorescent color of single-dopant white OLEDs. *Chem. Eur. J.*, **17** (2011), 13971-13977.

[67] K.E. Sapsford, L. Berti, I.L. Medintz, Materials for fluorescence resonance energy transfer analysis: beyond traditional donor–acceptor combinations. *Angew. Chem. Int. Ed.*, **45** (2006), 4562-4589.

[68] L.W. Chung, S. Hayashi, M. Lundberg, T. Nakatsu, H. Kato, K. Morokuma, Mechanism of efficient firefly bioluminescence via adiabatic transition state and seam of sloped conical intersection. *J. Am. Chem. Soc.*, **130** (2008), 12880-12881.

[69] L. Yue, Y.-J. Liu, W.-H. Fang, Mechanistic insight into the chemiluminescent decomposition of firefly dioxetanone. *J. Am. Chem. Soc.*, **134** (2012), 11632-11639.

[70] S.-F. Chen, I. Navizet, D. Roca-Sanjuán, R. Lindh, Y.-J. Liu, N. Ferré, Chemiluminescence of coelenterazine and fluorescence of coelenteramide: a systematic theoretical study. *J. Chem. Theory Comput.*, **8** (2012), 2796-2807.

[71] B.-W. Ding, Y.-J. Liu, Bioluminescence of firefly squid via mechanism of single electron-transfer oxygenation and charge-transfer-induced luminescence. *J. Am. Chem. Soc.*, **139** (2017), 1106-1119.

[72] M.-Y. Wang, Y.-J. Liu, Chemistry in fungal bioluminescence: a theoretical study from luciferin to light emission. *J. Org. Chem.*, **86** (2021), 1874-1881.

[73] V.N. Petushkov, B.G. Gibson, A.J.W.G. Visser, J. Lee, Purification and ligand exchange protocols for antenna proteins from bioluminescent bacteria, in: Methods Enzymol., Academic Press, 2000, 164-180.

[74] M. Kurfuerst, P. Macheroux, S. Ghisla, J. Woodland Hastings, Isolation and characterization of the transient, luciferase-bound flavin-4a-hydroxide in the bacterial luciferase reaction. *Biochim. Biophys. Acta, Gen. Subj.*, **924** (1987), 104-110.

[75] S.K. Cushing, J. Li, F. Meng, T.R. Senty, S. Suri, M. Zhi, M. Li, A.D. Bristow, N. Wu, Photocatalytic activity enhanced by plasmonic resonant energy transfer from metal to semiconductor. *J. Am. Chem. Soc.*, **134** (2012), 15033-15041.

[76] M. Wang, B. Bangalore Rajeeva, L. Scarabelli, E.P. Perillo, A.K. Dunn, L.M. Liz-Marzán, Y. Zheng, Molecular-fluorescence enhancement via blue-shifted plasmon-induced

DOI https://doi.org/10.4208/cicc.2025.71.01 | Generated on 2025-05-27 10:27:01

resonance energy transfer. *J. Phys. Chem. C*, **120** (2016), 14820-14827.

[77] Bavali, P. Parvin, S.Z. Mortazavi, S.S. Nourazar, Laser induced fluorescence spectroscopy of various carbon nanostructures (GO, G and nanodiamond) in Rd6G solution. *Biomed. Opt. Express,* **6** (2015), 1679-1693.

[78] J. Li, S.K. Cushing, F. Meng, T.R. Senty, A.D. Bristow, N. Wu, Plasmon-induced resonance energy transfer for solar energy conversion. *Nat. Photonics*, **9** (2015), 601-607.

[79] J. Lee, D.J. O'Kane, B.G. Gibson, Dynamic fluorescence properties of the bacterial luciferase intermediates. *Biochemistry*, **27** (1988), 4862-4870.

[80] T. Kulinski, A.J.W.G. Visser, D.J. O'Kane, J. Lee, Spectroscopic investigations of the single tryptophan residue and of riboflavin and 7-oxolumazine bound to lumazine apoprotein from Photobacterium leiognathi. *Biochemistry*, **26** (1987), 540-549.

[81] E.V. Nemtseva, N.S. Kudryasheva, The mechanism of electronic excitation in the bacterial bioluminescent reaction. *Russ. Chem. Rev.*, **76** (2007), 91-100.

DOI https://doi.org/10.4208/cicc.2025.71.01 | Generated on 2025-05-27 10:27:01